RESEARCH ARTICLE | JULY 18 2025

Adaptive excitation frequencies in simulations of resonance Raman spectra

James R. Cheeseman ; Petr Bouř

J. Chem. Phys. 163, 034118 (2025)
https://doi.org/10.1063/5.0274585

The Journal of Chemical Physics ARTICLE pubs.aip.org/aip/jcp

Adaptive excitation frequencies in simulations of resonance Raman spectra

Cite as: J. Chem. Phys. 163, 034118 (2025); doi: 10.1063/5.0274585
Submitted: 7 April 2025 • Accepted: 28 June 2025 •
Published Online: 18 July 2025

James R. Cheeseman[1] and Petr Bouř[2,a)]

AFFILIATIONS

[1] Gaussian Inc., 340 Quinnipiac St., Bldg. 40, Wallingford, Connecticut 06492-4050, USA
[2] Institute of Organic Chemistry and Biochemistry, Academy of Sciences, Flemingovo náměstí 2, 16610 Prague, Czech Republic

[a)] **Author to whom correspondence should be addressed:** bour@uochb.cas.cz

ABSTRACT

Within the Born–Oppenheimer approximation, differences of the vibrational energies are often neglected compared to the electronic ones. This leads to the Placzek approximation and the coupled-perturbed methodology, where the transition polarizabilities needed to simulate Raman spectra are calculated at an incident frequency. Within this approximation, the frequency change of the outgoing radiation is neglected, which has a little effect on the simulation of Raman and Raman optical activity spectra in the far from resonance limit. For resonance and pre-resonance, when the incident frequency is close to the energy of an electronic transition, significant error may arise. We analyze this problem and suggest a partial solution through a modification of the polarizability expressions to include a dependence on the vibrational frequencies. For model cobalt complexes, this improved formulation leads to a significant improvement of the spectral patterns.

INTRODUCTION

Resonance Raman scattering (RRS) has become a useful analytical method with many applications in chemistry and biology.[1–6] Recently, resonance Raman optical activity (RROA) has seen an increase in use due to theoretical developments[7–9] and the establishment of an experimental protocol, which separates the RROA signal from the ECD-Raman effect.[10,11]

The interpretation of the spectra is typically not straightforward. Spectral intensities depend on molecular transition polarizability expressions obtained from Dirac's time-dependent perturbation theory,[12,13] which contain unlimited summations over all excited molecular states. Within the Born–Oppenheimer (BO) and Placzek approximations, vibrational and electronic states can be treated separately.[14,15] The polarizabilities can be computed either as sums over states (SOSs)[16] or from time-dependent (TD) expressions[17–19] obtained using Fourier transformation to replace the summation over the vibrational states.

The SOS and TD approaches, however, are not practical in the general case where many electronic states contribute to the spectra.[16,20] Fortunately, in many instances when the contributions of particular vibrational states are not dominant, the summation over vibrational states can be replaced by the introduction of an effective bandwidth.[11,21,22] Using Placzek's idea, the transition polarizabilities are obtained from polarizability derivatives with respect to nuclear coordinates. These derivatives are available in common quantum chemical programs, which calculate Raman intensities within the HF, MP2, and DFT theories.[23–25] However, some of the adopted approximations, such as ignoring the dependence of the electronic energy on vibrational coordinates, may not be valid for the case of resonance.[26]

In the present study, we focus on a similar problem, as neglecting the vibrational states makes the polarizability derivatives asymmetric with respect to the excitation (incident) and scattered frequencies. This asymmetry is expected to have a particularly large effect on the RRS and RROA bands of higher-frequency vibrations. We analyze the theory in detail, demonstrate the error introduced in the spectra, and discuss the performance of ad hoc symmetrized polarizabilities.

THEORY

Following the generally accepted theory of Raman scattering, the incoming radiation electromagnetic field induces a molecular electric dipole that is the source of the scattered field.[27] The dynamic (time-dependent) dipole is proportional to the electric field and

transition polarizability. The polarizability can be obtained from the Schrödinger equation and the time-dependent perturbation theory. Resultant Raman intensities thus depend on the transition polarizabilities. The polarizability related to a transition from state i to state f is[7,27,28]

$$\alpha_{\alpha\beta}(i \to f) = \frac{1}{\hbar}\sum_{e\neq i,f}\left(\frac{\langle f|\mu_\alpha|e\rangle\langle e|\mu_\beta|i\rangle}{\omega_{ei}-\omega-i\Gamma_e} + \frac{\langle f|\mu_\beta|e\rangle\langle e|\mu_\alpha|i\rangle}{\omega_{ef}+\omega+i\Gamma_e}\right), \quad (1)$$

where $\hbar$ is the reduced Planck constant, the sum goes over excited states e, ω is the excitation frequency, $\boldsymbol{\mu}$ is the electric dipole moment operator, $\omega_{ei} = \omega_e - \omega_i$ and $\omega_{ef} = \omega_e - \omega_f$ are differences of the state frequencies, and Γ_e is the bandwidth.

In order to calculate Raman optical activity (ROA), except for the electric dipole, one has to consider the induced magnetic dipole and electric quadrupole moments. Four additional transition polarizabilities are then needed,[13]

$$G_{\alpha\beta} = \frac{1}{\hbar}\sum_{e\neq i,f}\frac{\langle f|\mu_\alpha|e\rangle\langle e|m_\beta|i\rangle}{\omega_{ei}-\omega-i\Gamma_e} + \frac{1}{\hbar}\sum_{e}\frac{\langle f|m_\beta|e\rangle\langle e|\mu_\alpha|i\rangle}{\omega_{ef}+\omega+i\Gamma_e}, \quad (2a)$$

$$\mathcal{G}_{\alpha\beta} = \frac{1}{\hbar}\sum_{e\neq i,f}\frac{\langle f|m_\alpha|e\rangle\langle e|\mu_\beta|i\rangle}{\omega_{ei}-\omega-i\Gamma_e} + \frac{1}{\hbar}\sum_{e}\frac{\langle f|\mu_\beta|e\rangle\langle e|m_\alpha|i\rangle}{\omega_{ef}+\omega+i\Gamma_e}, \quad (2b)$$

$$A_{\alpha,\beta\gamma} = \frac{1}{\hbar}\sum_{e\neq i,f}\frac{\langle f|\mu_\alpha|e\rangle\langle e|\Theta_{\beta\gamma}|i\rangle}{\omega_{ei}-\omega-i\Gamma_e} + \frac{1}{\hbar}\sum_{e}\frac{\langle f|\Theta_{\beta\gamma}|e\rangle\langle e|\mu_\alpha|i\rangle}{\omega_{ef}+\omega+i\Gamma_e}, \quad (2c)$$

$$\mathcal{A}_{\alpha,\beta\gamma} = \frac{1}{\hbar}\sum_{e\neq i,f}\frac{\langle f|\Theta_{\beta\gamma}|e\rangle\langle e|\mu_\alpha|i\rangle}{\omega_{ei}-\omega-i\Gamma_e} + \frac{1}{\hbar}\sum_{e}\frac{\langle f|\mu_\alpha|e\rangle\langle e|\Theta_{\beta\gamma}|i\rangle}{\omega_{ef}+\omega+i\Gamma_e}, \quad (2d)$$

where $\mathbf{m}$ and $\boldsymbol{\Theta}$ are operators of the magnetic dipole moment and electric quadrupole moment, respectively. As for $\boldsymbol{\alpha}$, these tensors are in general complex. Note also that the magnetic dipole moment operator is purely imaginary, while $\boldsymbol{\mu}$ and $\boldsymbol{\Theta}$ are real. Only for $\Gamma_e = 0$ and real wave functions, $\boldsymbol{\alpha}$, $\mathbf{A}$, and $\mathcal{A}$ are real, while $\mathbf{G}$ and $\mathcal{G}$ are imaginary, which may simplify practical computations.

Let us focus on Eq. (1) as the reasoning for expressions (2a)–(2d) is similar. Raman intensity depends on a concrete experimental setup. In general, it is a combination of three terms,[29]

$$I = K_0\alpha^s_{\alpha\alpha}\alpha^{s*}_{\beta\beta} + K_s\alpha^s_{\alpha\beta}\alpha^{s*}_{\alpha\beta} + K_a\alpha^a_{\alpha\beta}\alpha^{a*}_{\alpha\beta}, \quad (3)$$

where K_0, K_s, and K_a are constants, the Einstein summation convention is used, $\alpha^s_{\alpha\beta} = (\alpha_{\alpha\beta} + \alpha_{\beta\alpha})/2$ is the symmetric polarizability part, and $\alpha^a_{\alpha\beta} = (\alpha_{\alpha\beta} - \alpha_{\beta\alpha})/2$ is the anti-symmetric polarizability part. Similarly, ROA intensities are proportional to products of the polarizability $\boldsymbol{\alpha}$ with complex-conjugate symmetrized and anti-symmetrized tensors $\mathbf{G}$ and $\mathbf{G}$ and reduced forms of $\mathbf{A}$ and $\mathbf{A}$.[29]

We would like to investigate the intensities for a forward ($i \to f$, excitation frequency ω, scattered frequency ω') and a backward ($f \to i$, excitation frequency ω', scattered frequency ω) transition. From Eq. (1) and a simple manipulation, we get

$$\alpha^{s/a}_{\alpha\beta}(i \to f) = \frac{1}{2\hbar}\sum_{e\neq i,f}\left(\langle f|\mu_\alpha|e\rangle\langle e|\mu_\beta|i\rangle \pm \langle f|\mu_\beta|e\rangle\langle e|\mu_\alpha|i\rangle\right) \times\left(\frac{1}{\omega_{ei}-\omega-i\Gamma_e} \pm \frac{1}{\omega_{ef}+\omega+i\Gamma_e}\right), \quad (4)$$

$$\alpha^{s/a}_{\alpha\beta}(f \to i) = \frac{1}{2\hbar}\sum_{e\neq i,f}\left(\langle i|\mu_\alpha|e\rangle\langle e|\mu_\beta|f\rangle \pm \langle i|\mu_\beta|e\rangle\langle e|\mu_\alpha|f\rangle\right) \times\left(\frac{1}{\omega_{ef}-\omega'-i\Gamma_e} \pm \frac{1}{\omega_{ei}+\omega'+i\Gamma_e}\right). \quad (5)$$

Using symmetry of the transition matrix elements, $\langle e|\mu_\alpha|i\rangle = \langle i|\mu_\alpha|e\rangle$, and realizing that $\omega_{ef} - \omega' = \omega_{ei} - \omega$ and $\omega_{ef} + \omega = \omega_{ei} + \omega'$, we see that expressions (4) and (5) are equal in absolute values, giving the same intensities,

$$I(i \to f) = I(f \to i). \quad (6)$$

Within the BO approximation, we may neglect vibrational frequencies in the denominator and write each state as a product of electronic and vibrational parts, e.g., $|e\rangle = |e_e\rangle|e_v\rangle$. Using the resolution of the identity, $\sum_v |e_v\rangle\langle e_v| = 1$, $\boldsymbol{\alpha}$ becomes symmetric ($\alpha^a_{\alpha\beta} = 0$), and we get

$$\alpha_{\alpha\beta}(n \to m) = \frac{1}{\hbar}\sum_{e\neq i}\langle m|\mu_{e0,\alpha}\mu_{e0,\beta}|n\rangle \times\left(\frac{1}{\omega_{e0}-\omega-i\Gamma_e} + \frac{1}{\omega_{e0}+\omega'+i\Gamma_e}\right), \quad (7a)$$

$$\alpha_{\alpha\beta}(m \to n) = \frac{1}{\hbar}\sum_{e\neq i}\langle n|\mu_{e0,\alpha}\mu_{e0,\beta}|m\rangle \times\left(\frac{1}{\omega_{e0}-\omega'-i\Gamma_e} + \frac{1}{\omega_{e0}+\omega+i\Gamma_e}\right), \quad (7b)$$

where we now use the letter e for electronic excited states, the elements $\mu_{e0,\alpha} = \langle e_e|\mu_{e0,\alpha}|0_e\rangle$ contain excited e_e and ground 0_e electronic states, n and m are, respectively, the initial and final vibrational states, and ω_{e0} is the difference of the excited and ground electronic energies. In this case, $I(n \to m) \neq I(m \to n)$ as far as $\omega \neq \omega'$. In other words, condition (6) is not met. This is, of course, a fundamental problem. In the dark, if the transition probabilities are not equal, due to the vacuum excitations,[30] the system would be spontaneously pumped into one state or another. In addition, within the classical mechanical approach, the molecule is supposed to behave symmetrically with respect to the incoming and outgoing radiation.[31] While in the FFR case, polarizabilities (7a) and (7b) are close, they diverge more in resonance or pre-resonance when ω or ω' approaches ω_{e0}.

To partially rectify this inconsistency, we consider the polarizability expression with the excitation frequency dependent on the frequency ω_{nm} of each vibrational transition $n \to m$. For simplicity, we use a uniform width $\Gamma_\varepsilon = \Gamma$ in the calculations. Considering fundamental transitions of vibrational mode I, $\omega_{nm} = \omega_I$ is the fundamental frequency, and we use the average, $\overline{\omega}_I = (\omega + \omega')/2 = \omega - \omega_I/2$, so that

$$\alpha_{\alpha\beta}(0 \to I) = \frac{1}{\hbar}\sum_{e\neq i}\langle I|\mu_{e0,\alpha}\mu_{e0,\beta}|0\rangle\left(\frac{1}{\omega_{e0}-\overline{\omega}_I-i\Gamma} + \frac{1}{\omega_{e0}+\overline{\omega}_I+i\Gamma}\right), \quad (8)$$

satisfying condition (6). Otherwise, we use the usual Placzek approximation[15] where the transition polarizability is expressed as

$$\alpha_{\alpha\beta}(0 \to I) = \frac{\partial\alpha^e_{\alpha\beta}}{\partial Q_I}(\overline{\omega}_I)\sqrt{\frac{\hbar}{2\omega_I}}, \quad (9)$$

where $\alpha^{e}_{\alpha\beta}(\omega) = \frac{1}{\hbar}\sum_{e\neq i}\mu_{e0,\alpha}\mu_{e0,\beta}\left(\frac{1}{\omega_{e0}-\omega-i\Gamma} + \frac{1}{\omega_{e0}+\omega+i\Gamma}\right)$ is the electronic (non-transition) polarizability. Within the coupled-perturbed DFT methodology, the summations over the excited states are implicit, and the polarizabilities and their derivatives are calculated as analytic energy derivatives [e.g., $\alpha^{e}_{\alpha\beta} = -(1/2)\partial^2\varepsilon/\partial E_\alpha/\partial E_\beta$, where ε is the energy and $E = E(\omega)$ is the electric intensity].[11,21,25] Typically, the derivatives of **α** and the ROA polarizabilities are evaluated at the optimized geometry, to be consistent with the harmonic approximation for vibrational frequencies.

COMPUTATIONS

The CoEDDS and BuCo cobalt complexes (Fig. 1) were chosen as model systems, for which high-quality experimental RRS and RROA spectra at 532 nm excitation are available.[16,20] CoEDDS has a strong $S_0 \rightarrow S_3$ transition in the vicinity of the 532 nm laser line, lower-energy $S_0 \rightarrow S_1$ and $S_0 \rightarrow S_2$ transitions are weak, and all others occur below 410 nm. For BuCo, the absorption threshold starts approximately at 532 nm, but many transitions occur above and below it. Experimental and calculated absorption and electronic circular dichroism spectra of CoEDDS and BuCo can be found in Refs. 16 and 20, respectively.

Both compounds also possess C_2 symmetry and are relatively rigid, which enhances treatment at a relatively high approximation level. A development version of the Gaussian software[32] was used for the quantum-chemical computations. For optimized geometries, complex polarizability derivatives were computed analytically at several excitation wavelengths so that the adapted excitation frequencies for each vibrational normal mode could be obtained by interpolation, using a third-order polynomial fitting. The bandwidth was chosen on the basis of UV–Vis absorption spectra as $\Gamma = 880\ \mathrm{cm}^{-1}$. For BuCo, the B3LYP/6-311++G(2d,p)/PCM($CHCl_3$) level of theory was applied and CoEDDS was treated at the B3LYP(or B3PW91)/6-311++G(2d,p)/PCM(H_2O) level (ROA vacuum only). Note that, within the Placzek approximation, $\mathcal{G}_{e,\alpha\beta} = -G_{e,\beta\alpha}$ and $\mathcal{A}_{e,\alpha,\beta\gamma} = A_{e,\alpha,\beta\gamma}$ so that only three tensors are needed to simulate the Raman and ROA intensities. Scattered circular polarization (SCP) backscattering (180°) Raman and ROA intensities were then obtained at the harmonic level using the working equations,

$$I_{Raman} = \mathrm{Re}(\alpha^{s}_{\alpha\alpha}\alpha^{s*}_{\beta\beta} + 7\alpha^{s}_{\alpha\beta}\alpha^{s*}_{\alpha\beta}), \tag{10}$$

$$I_{ROA} = 8\ \mathrm{Im}\left[3\alpha^{s}_{\alpha\beta}G^{s*}_{\alpha\beta} - \alpha^{s}_{\alpha\alpha}G^{s*}_{\beta\beta} + \frac{1}{3}i\omega\alpha^{s}_{\alpha\beta}(\varepsilon_{\alpha\gamma\delta}A^{*}_{\gamma,\delta\beta})^{s}\right]. \tag{11}$$

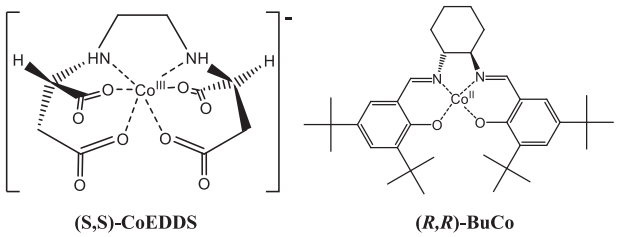

(S,S)-CoEDDS (*R*,*R*)-BuCo

FIG. 1. Structures of the (*S*,*S*)-N,N-ethylenediamine disuccinic cobalt(III) (**CoEDDS**) and (*R*,*R*)-(-)-N,N′-bis(3,5-di-tert-butylsalicylidene)-1,2-cyclohexanediamino cobalt(II) (**BuCo**) complexes.

For the intensities, smooth spectra were obtained by summing over normal modes (*i*) as

$$S(\nu) = \sum_i I_i\left[1 - \exp\left(-\frac{\nu_i}{kT}\right)\right]^{-1}\left[4\left(\frac{\nu-\nu_i}{\Delta}\right)^2 + 1\right]^{-1}, \tag{12}$$

where ν is the vibrational frequency, k is the Boltzmann constant, T is temperature, and $\Delta = 10\ \mathrm{cm}^{-1}$. Since absolute intensities are not measured, simulated spectra were normalized to experimental Raman areas.

RESULTS AND DISCUSSION

Frequency dependence of polarizability derivatives

Examples of the dependencies of derivatives of the α, G, and A tensors are shown in Fig. 2. For BuCo, they were calculated for 470, 475, 480, 485, 490, 500, 532, and 550 nm excitation wavelengths. The dependence is relatively monotonic and therefore reasonably reproduced by third-degree polynomials. While the α and A derivatives in the investigated interval do not change by more than a few percent, the G derivatives change more profoundly. This has a significant effect on ROA spectra, especially in (pre-)resonance, where in the extreme case of single electronic state limit, the contribution of A vanishes and the RROA intensities depend on G only.[8]

Simulations with fixed excitation frequency

For CoEDDS, RRS and RROA intensities were calculated for ten excitation wavelengths (510, 520, 525, 528, 530, 532, 540, 545, 550, and 580 nm), for both the B3LYP and B3PW91 functionals. Average errors with respect to the experiment are shown in Fig. 3. The two functionals give similar results, and spectra within 200–2000 cm^{-1} are best reproduced by excitation wavelength around 530 nm. However, the higher-frequency part of the spectrum (1000–2000 cm^{-1}) suggests that a better agreement would be achieved for longer excitation wavelengths, such as for those above 545 nm. This can be explained by the reasoning given above. For example, for 532 nm excitation, the scattered wavelength for a 200 cm^{-1} vibrational transition is 538 nm. However, for a 1500 cm^{-1} vibrational band, the scattered radiation wavelength is 578 nm. For such high-frequency bands, polarizabilities obtained at 532 nm are less realistic.

The effect of the frequency adaptation

In Fig. 4, we compare the Raman and ROA spectra of BuCo and CoEDDS in the higher-frequency region computed with and without the frequency adaption along with the experiment. The two compounds behave somewhat differently as they represent weakly and strongly resonating systems, respectively.

For BuCo (the upper part of the figure), the RROA spectrum itself is predominantly of positive sign, somewhat proportional to the Raman signal, which is in line with the single electronic state theory.[8] State number 8 was predicted as the critical one,[20] although more electronic transitions are involved, exact contributions of which may be predicted by DFT only approximately.[20] As expected, the low-wavenumber part of the spectra (~<1500 cm^{-1}) is not much affected by the frequency adaptation. In this region,

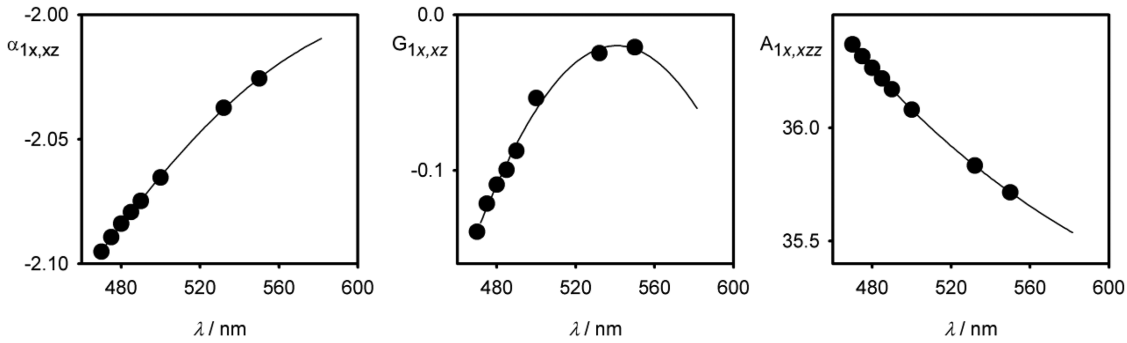

FIG. 2. Examples of the tensor derivatives calculated at eight excitation wavelengths, in atomic units; derivatives with respect to the *x*-coordinate of the first (metal) atom, $\partial\alpha_{xz}/\partial R^1_x$, $\partial G_{xz}/\partial R^1_x$, and $\partial A_{xzz}/\partial R^1_x$, BuCo, B3LYP/6-311++G(2d,p)/PCM/$CHCl_3$; the solid lines correspond to third-degree polynomial fits.

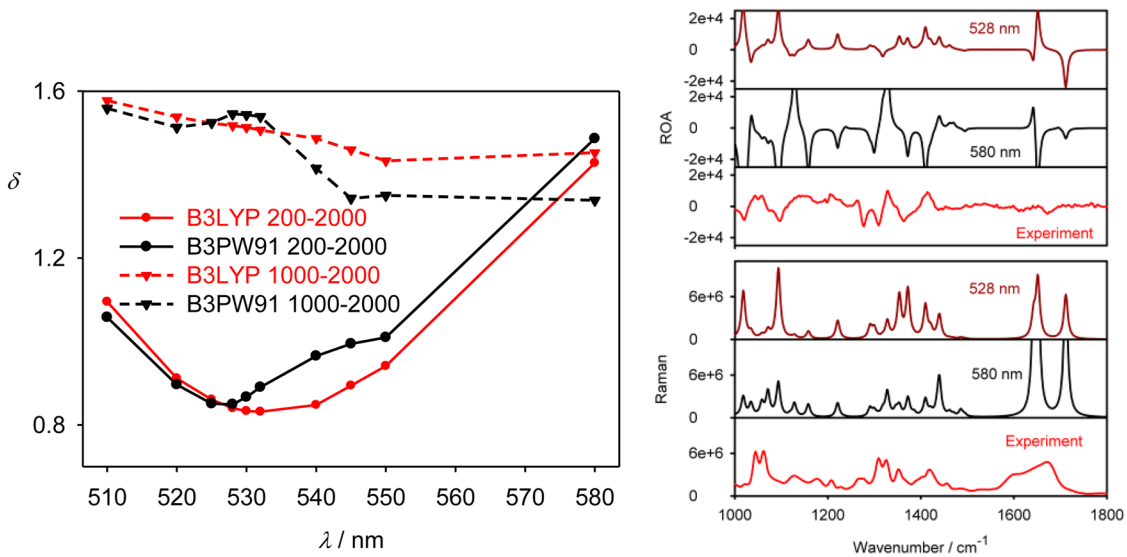

FIG. 3. CoEDDS: (left) error ($\delta = \int |S' - S'_{exp}| d\omega$) between normalized ($S' = S/\int |S| d\omega$) computed and experimental ROA spectra, for the B3LYP and B3PW91 functionals, ten excitation wavelengths, the 6-311++G(2d,p) basis set, and integrations within the 200–2000 and 1000–2000 cm^{-1} intervals; (right) example of spectral changes (B3PW91, 528 and 580 nm excitations).

we can see minor changes of Raman (~10%) and ROA (0%–20%) intensities. They are more pronounced for the 1600 cm^{-1} signal, where the Raman intensity drops by about 20%. For ROA, the adaptation reduces its intensity much more, by 50%, in closer agreement with the experiment. Interestingly, the average spectral similarities are not much affected; for Raman, the similarity is even slightly smaller after the adaptation. This points out limitations of the spectra comparisons based solely on mechanistic automatic criteria. The significant effect on the highest-wavenumber band suggests the importance of the frequency adaptation for more precise computations.

For the CoEDDS complex (the lower part of the figure), where the excitation frequency is much closer to the most contributing electronic transition ($S_0 \rightarrow S_3$),[16] the resonance is much stronger than for BuCo. Consequently, the effect of the frequency adaptation is much bigger, again leading to a closer agreement with the experiment. Even Raman spectra are notably improved in terms of the similarity, increasing from 65% to 70%. ROA simulated without the adaptation gives extremely poor similarity (5%) within the 900–1800 cm^{-1} interval, while more reasonable 34% is achieved with it. The resultant error may be attributed to the error of the force field, influence of the water environment not sufficiently represented by the dielectric models, and vibronic effects,[16] all of them going beyond the scope of the present study. In Fig. 4, particularly striking are the sign improvements, e.g., within 1600–1700 cm^{-1}, where instead of the strong bands of opposite sign, two weaker negative bands are obtained with the frequency-adaptation, in better agreement with the experiment. Similarly, experimental negative ROA

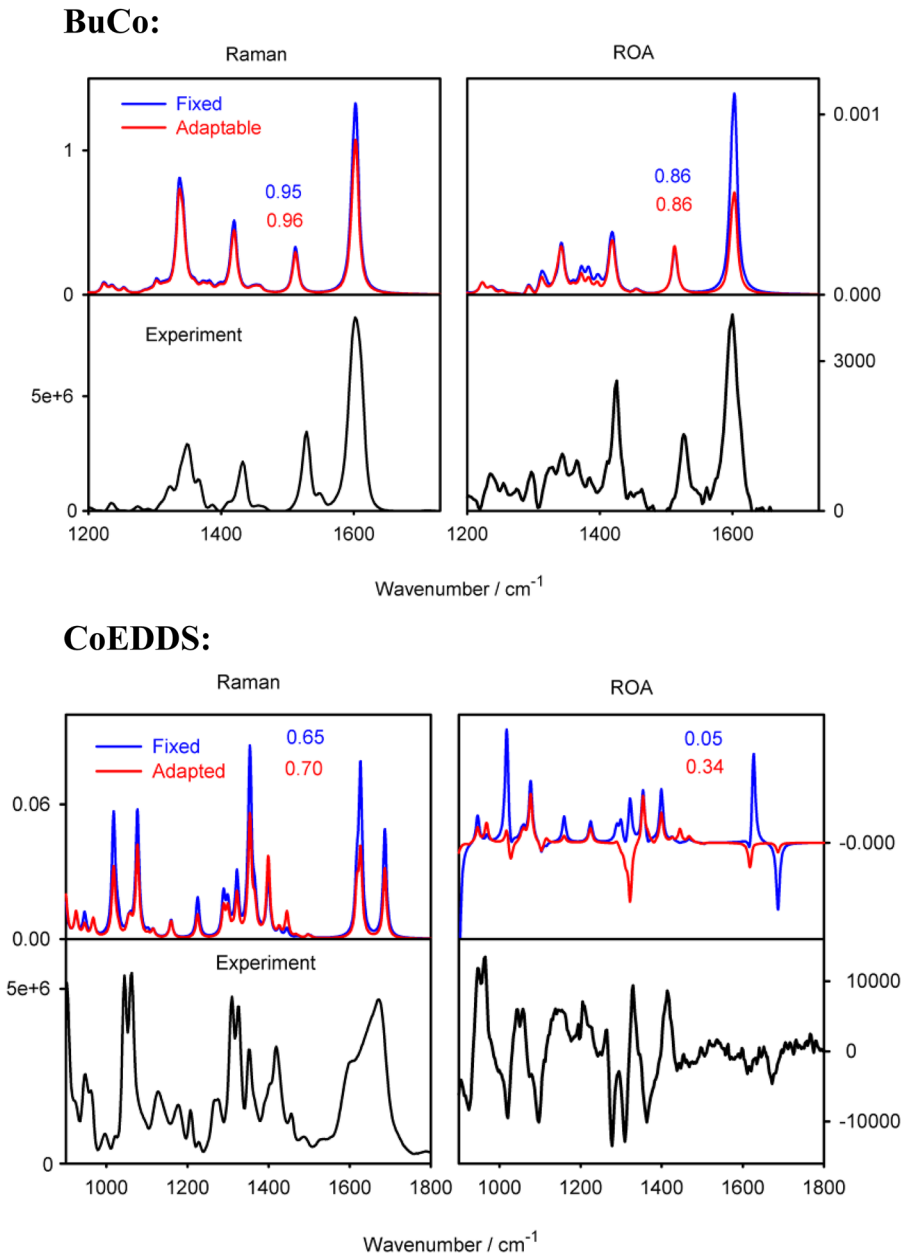

FIG. 4. BuCo and CoEDDS: simulated Raman and ROA spectra with fixed (532 nm, blue) and adaptable (red) excitation wavelength and the experiments. Similarity factors ($\int S'_{Sim} S'_{Exp} d\nu$ for spectra normalized as $S' = \sqrt{\int S^2 d\nu}$) are indicated, and calculated frequencies were multiplied by 0.973 for easier comparison. Details about the experimental data can be found in Refs. 16 and 20.

signal around 1300 cm^{-1} is reproduced only with the frequency adaptation.

In summary, the results shown above confirm the theoretical analysis and indicate that proper treatment of the excitation frequency in the calculation becomes important for a good reproduction of resonance or pre-resonance Raman and ROA spectra. The frequency adaptation for systems explored in the present study brought about a significant improvement compared to computations with fixed excitation frequency. However, it is likely that other factors contribute to the computational error. In this sense, we view the excitation frequency issue discussed above as a contribution to the theoretical apparatus of the relatively young resonance Raman and ROA spectroscopies and that this will enhance their applications in analytical chemistry and biochemical research.

CONCLUSIONS

The common way of computing Raman and ROA intensities, where only one excitation frequency is used for the whole vibrational spectrum, is appropriate for the far from resonance cases where the excitation frequency significantly differs from the frequencies of the electronic transitions. For pre-resonance and resonance, this

approach can lead to significant errors in the Raman and ROA intensities, which we could show by discussing both the theory and practical examples. Our proposed empirical vibrational frequency-adapted formulation leads to a significantly better agreement with respect to the experimental spectra for the two cobalt complexes studied here.

ACKNOWLEDGMENTS

This work was supported by the Grant Agency of the Czech Republic (Grant No. 25-15726S).

AUTHOR DECLARATIONS

Conflict of Interest

The authors have no conflicts to disclose.

Author Contributions

James R. Cheeseman: Investigation (equal); Software (equal); Writing – review & editing (equal). **Petr Bouř**: Investigation (equal); Software (equal); Writing – review & editing (equal).

DATA AVAILABILITY

The data that support the findings of this study are available within the article.

REFERENCES

[1] J. M. Benevides, S. A. Overman, and G. J. Thomas, J. Raman Spectrosc. **36**, 279 (2005).
[2] T. Holtum *et al.*, J. Raman Spectrosc. **52**, 2292 (2021).
[3] J. Dybas *et al.*, Analyst **143**, 3489 (2018).
[4] A. Ianoul *et al.*, J. Phys. Chem. A **106**, 3621 (2002).
[5] Z. Ahmed, N. S. Myshakina, and S. A. Asher, J. Phys. Chem. B **113**, 11252 (2009).
[6] R. J. H. Clark and T. J. Dines, Angew Chem. Int. Ed. Engl. **25**, 131 (1986).
[7] L. Nafie, *Vibrational Optical Activity: Principles and Applications* (Wiley, Chichester, 2011).
[8] L. A. Nafie, Chem. Phys. **205**, 309 (1996).
[9] G. Zając and P. Bouř, J. Phys. Chem. B **126**, 355 (2022).
[10] T. Wu *et al.*, Angew. Chem. Int. Ed. **59**, 21895 (2020).
[11] G. Li *et al.*, Angew. Chem. Int. Ed. **60**, 22004 (2021).
[12] P. A. M. Dirac, *The Principles of Quantum Mechanics* (Cambridge University Press, Cambridge, 1930).
[13] L. D. Barron, *Molecular Light Scattering and Optical Activity* (Cambridge University Press, Cambridge, 2004).
[14] M. Born and R. Oppenheimer, Ann. Phys. **84**, 457 (1927).
[15] G. Placzek, in *Handbuch der Radiologie*, edited by E. Marx (Akademische Verlagsgesellschaft, Leipzig, 1934), p. 205.
[16] Q. Yang *et al.*, Angew. Chem. Int. Ed. **62**, e202312521 (2023).
[17] A. Baiardi, J. Bloino, and V. Barone, J. Chem. Phys. **141**, 114108 (2014).
[18] F. Egidi *et al.*, J. Chem. Theory Comput. **10**, 346 (2014).
[19] A. Baiardi, J. Bloino, and V. Barone, J. Chem. Theory Comput. **14**, 6370 (2018).
[20] T. Wu, J. Kapitán, and P. Bouř, J. Phys. Chem. Lett. **13**, 3873 (2022).
[21] L. Jensen *et al.*, J. Chem. Phys. **127**, 134101 (2007).
[22] L. Jensen *et al.*, J. Chem. Phys. **123**, 174110 (2005).
[23] J. A. Pople *et al.*, Int. J. Quantum Chem. **16**, 225 (1979).
[24] A. G. Ioannou and R. D. Amos, Chem. Phys. Lett. **279**, 17 (1997).
[25] P. Norman, K. Ruud, and T. Saue, *Principles and Practices of Molecular Properties* (Wiley, Oxford, 2018).
[26] J. Šebestík and P. Bouř, Phys. Rev. A **111**, 062804 (2025).
[27] D. A. Long, *The Raman Effect: A Unified Treatment of the Theory of Raman Scattering by Molecules* (Wiley, Chichester, 2002).
[28] R. Dick, in *Advanced Quantum Mechanics*, edited by R. Dick (Springer, Cham, Switzerland, 2020).
[29] L. Hecht and L. A. Nafie, Mol. Phys. **72**, 441 (1991).
[30] D. P. Craig and T. Thirunamachandran, *Molecular Quantum Electrodynamics* (Dover Publications, New York, 1998).
[31] J. Kessler and P. Bouř, J. Chem. Theory Comput. **18**, 1780 (2022).
[32] M. J. Frisch *et al.*, Gaussian Development Version, Revision J.30+ (Wallingford CT, 2022).